ARMY RESEARCH LABORATORY

An Investigation of the Erosion Physics/Mechanisms of Current Army Systems (Point Studies)

by Paul J. Conroy, Paul Weinacht,
and Michael J. Nusca

ARL-TR-2054   September 1999

19991101 039

DTIC QUALITY INSPECTED 4

Army Research Laboratory
Aberdeen Proving Ground, MD 21005-5066

ARL-TR-2054   **September 1999**

An Investigation of the Erosion Physics/Mechanisms of Current Army Systems (Point Studies)

Paul J. Conroy, Paul Weinacht, and Michael J. Nusca
Weapons and Materials Research Directorate, ARL

Abstract

Future systems performance requirements have led to a heightened awareness of the erosion issue and to the development of erosion investigations in the U.S. Army and Navy. These investigations involve experimental and modeling efforts to understand the thermal, chemical, and mechanical contributions to erosion/wear. A description of the mechanistic erosion representation follows in this report. The calculation procedure is illustrated, including details of the mass transport scheme, gas surface interface, surface melt wipe model with dynamic gridding, and the equilibrium kinetics model, which utilizes the NASA Lewis thermochemcial library.

The following cartridges are investigated: the M829A2 APFSDS in the M256 120-mm tank cannon and the M791-APDS-T and 616W-APFS (the "original" M919), both in the 25-mm Bushmaster cannon. The resulting mass lost per round for these systems compares well qualitatively with the experimental data, providing some support to the assumptions in the code. The primary conclusion is that carburization leading to iron carbide formation is an important contributing factor for much of the material lost from the steel barrel once it is exposed through cracks or chips in the surface coating.

Table of Contents

INTENTIONALLY LEFT BLANK.

List of Figures

INTENTIONALLY LEFT BLANK.

1. Introduction

System performance demands are forcing changes in gun tubes in the areas of pressure limits, length, firing rate, and erosion resistance. This has created a resurgence of the interest in gun tube erosion and the associated mechanisms. Historically, the propellant adiabatic flame temperature was used as an indicator of the erosivity of a propellant. Unfortunately, flame temperature is not the only factor [1, 2] influencing the erosion process, which includes mechanical abrasion, pyrolysis, melting, and spalling. Also, once the erosion rate was predicted using the flame temperature correlations, understanding what could be done to mitigate the erosion was left a mystery with the exception of the obvious solution of applying surface coatings or ablatives.

The effectiveness of surface coatings depends upon the ability of the coating to block the thermal and chemical attack of the propellant combustion products with the gun bore surface. Permanent tube coatings, such as chromium, have been successfully implemented in both artillery and direct-fire systems. One concern for the use of chromium as a coating is that the hexavalent state used in electroplating is environmentally undesirable to the level that one day it may be eliminated as a design option. Many other coatings, such as functionally gradient coatings and ceramic coatings, although unsuccessful in the past, are continuously being examined as possible candidates [3]. Also being examined are refractory metals, such as rhenium, molybdenum, niobium, and tantalum, of which tantalum appears to be the optimal choice [4]. Much effort is being placed in coating process technology for these materials by various elements of the Army and Navy. Successful implementation of propelling charge additives, such as talc, TiO_2, waxes, greases, and combinations thereof, that deposit on the tube or in the boundary layer and act as coatings are usually Edisonian in nature and without knowledge of the mechanisms of how or why one additive works better than another.

Attempts to model erosion using first principles have been and are currently being made [5–8], although it is believed that significant additional work is still required to understand the fundamental

1

physics involved. In this report the possible mechanisms will be elaborated upon and then applied to specific systems.

2. Mechanistic Description

A modular treatment of the contributing factors to erosion consisting of three fully coupled portions, to include thermal ablation with an iterative solution for the surface regression; independent heat and multicomponent species mass transport to the surface; and full equilibrium thermochemistry was utilized. The contributions due to mechanical wear and abrasion, however, are not included. A surface control volume treatment ensures conservation of mass. The gas-phase properties in the core flow of the gun tube from the XKTC [9] or NGEN [10] interior ballistic codes are used in the calculations, as well as species data from IBBLAKE [11–13] or NGEN. The thermochemistry calculation incorporates the NASA Lewis [14] thermochemical database.

Primary features include:

- Variable surface thermo-physical properties: specific heat C_p and conductivity k.

- Surface material phase change from base-centered cubic (BCC) to face-centered cubic (FCC). The material replenishment section recognizes the surface temperature and the correct phase. There are no phase change hysteresis nor are there two-phase (BCC+FCC) regions.

- A user-defined "freeze-out" temperature to enable the surface chemistry portion.

- A user selection for two-phase control volume temperature: (1) Surface temperature and (2) a mixture control volume temperature with both gas- and solid-phase contributions.

- User-defined surface materials, both reactant and product species.

2

- A user-defined surface coating - if any.

- No hardwired inputs. All primary inputs are user defined.

The following assumptions are in the model:

- One-dimensional (1-D) heat conduction.

- Subsurface 1-D diffusion only of carbon.

- All surface liquids and gas products are removed.

- No feedback to the interior ballistics calculation in the core flow.

- Released chemical energy treated as a source term.

- Species are chemically frozen from core flow to the wall.

The description, shown conceptually in Figure 1, enables the surface to heat convectively until the user-defined freeze-out temperature is overcome. At this point, the control volume at the surface is defined and supplied with species from the mass transport routines. Surface reactions are then permitted to occur, which release additional energy into the system as a surface source term and produce various gas, solid, or liquid products. The reaction products can be either unvaried, as some solid materials, or be removed from the area as liquids or gases. The latter case results in pyrolysis or ablation. As the surface regresses, the solids are refreshed accordingly with fresh steel.

Preliminary calculations must be made using interior ballistic codes to provide the core flow state variables of temperature and pressure as well as the velocity and the species concentrations. These outputs are then used as input along with a user-defined input file to the calculation.

3
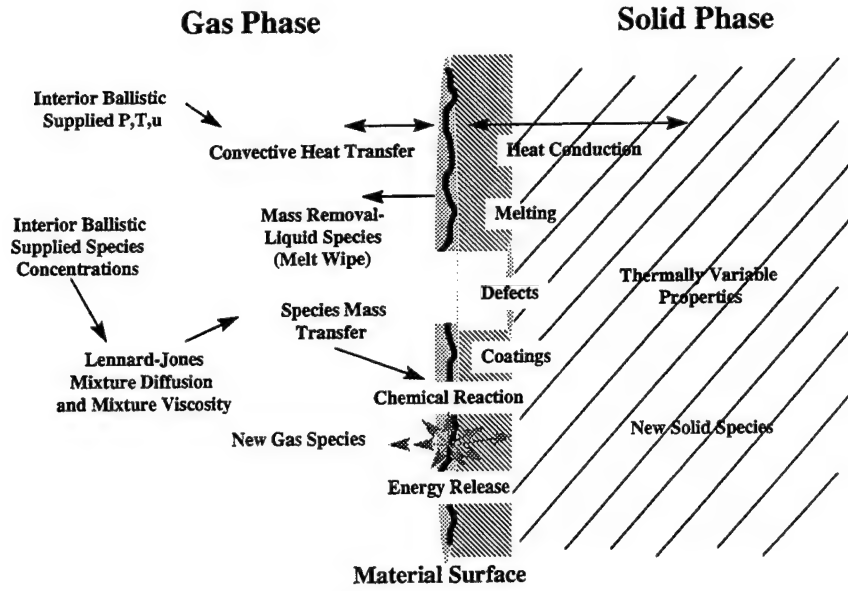
Figure 1. Conceptual Erosion Description.

3. Ablation-Conduction Model and Computational Approach

The in-depth temperature response, T(r), of the unablated (solid) material is modeled using the 1-D heat conduction equation as follows:

$$\rho C_p \frac{\partial T}{\partial t} = \frac{1}{r^\beta} \frac{\partial}{\partial r}\left(r^\beta k \frac{\partial T}{\partial r}\right). \tag{1}$$

By setting $\beta = 0$ or $\beta = 1$, the planar or axisymmetric form of the governing equation can be obtained. In this form of the equation, the relevant material properties are density, ρ, specific heat, C_p, and conductivity, k. The conductivity and specific heat may vary but must remain continuous.

4

The surface (heat) energy balance, while gross melting is not occurring, includes the convective heat input to the surface along with the possible contribution due to the surface reaction, shown in equation 2. This source term is balanced with the energy conducted through the material.

$$h\left(T_{gas} - T_{wall} \right) = -k\frac{\partial T}{\partial r} - source \tag{2}$$

However, when the system is melting, the energy balance also includes the fixed-surface temperature condition and the unknown surface location. The surface temperature cannot rise beyond the specified melting value because any additional energy is applied to the latent heat of formation of the molten material, as shown in equations 3 and 4, where S_{surf} is the surface location:

$$T_{wall} = T_{melt} \tag{3}$$

$$\rho L \frac{\partial S_{surf}}{\partial t} = h\left(T_{gas} - T_{wall} \right) + k\frac{\partial T}{\partial r} - Source. \tag{4}$$

To provide closure for the in-depth temperature response of the gun tube, a convective boundary condition is applied to the outer surface of the gun tube.

$$h_{amb}\left(T_{outer-wall} - T_{\infty} \right) = -k\frac{\partial T}{\partial r} \tag{5}$$

The governing equations and boundary conditions are solved using a Crank-Nicholson finite-difference technique. Prior to the onset of melting, the governing equations and boundary conditions are linear and solutions are obtained in a direct (noniterative) fashion. During the melting process, the equations become nonlinear since the dimensions of the computational domain are coupled with the regression rate. An iterative approach is utilized during melting to appropriately address the nonlinearity.

Because the boundary of the computational domain moves during the erosion event, a transformed version of the governing equation is employed. This allows the equations to be solved in a fixed computational space even though the physical boundary is moving. A generalized

5

transformation between the computational coordinate, ξ, and the physical coordinate, r, is utilized. The transformed equations are shown below.

$$\rho C_p \left(\frac{\partial T}{\partial t} + \xi_t \frac{\partial T}{\partial \xi} \right) = \frac{1}{r} \xi_r \frac{\partial}{\partial \xi} \left(rk\xi_r \frac{\partial T}{\partial \xi} \right)$$

$$\xi_t = \frac{-r_t}{r_\xi} \equiv \frac{\partial r}{\partial t} \frac{\partial \xi}{\partial r}$$

$$\xi_r = \frac{1}{r_\xi} \equiv \frac{\partial \xi}{\partial r}$$

(6)

In this form, the nonlinear nature of the governing equation produced by the moving boundary is evident because the metric terms, ξ_r and ξ_t, are not constant and are dependent on the erosion rate when the grid is moving.

This methodology compares very well to the semianalytical solutions of Landau [15] in test cases [7].

4. Heat Transport to Surface

The heat flux to the surface is provided through convective heat transport and energy release as shown [16, 17].

$$Q_w = 0.037 \frac{\mu^*}{\chi} Re^{*0.8} \frac{C_f}{C_{f_i}} C_p \left(T_g - T_w \right),$$

(7)

where $\dfrac{C_f}{C_{f_i}}$ is the compressible skin friction ratio, Re^* is the compressible Reynolds number, μ^* is the viscosity, χ is a pressure normalized length scale from the entrance region, C_p is the specific heat of the gases, and T_g and T_w are the gas temperature and wall temperature, respectively.

6

This heat flux reduces to the following boundary condition imposed upon the inner wall:

$$-k\frac{\partial T}{\partial r} = h_{conv}\left(T_g - T_w\right) + source.$$ (8)

This boundary condition has been modified for erosion studies with the incorporation of surface defects primarily in coated gun tubes. This has been done by using the ratio of the Stanton numbers (Nusselt/Reynolds/Prandtl) for smooth and rough tubes, defined by the depth of the pit. The frictional factor may be computed by solving Colbrook's function [18], as shown in equation 9.

$$f^{-1/2} = -2\log\left(\frac{e/D}{3.7} + \frac{2.51}{\sqrt{f}\,Re_D}\right),$$ (9)

with e the depth of the defect, D the bore diameter, and Re_D the Reynolds number. The computation of the Stanton number for rough and smooth surfaces can be performed through the following set of equations and instructions in the *Handbook of Single-Phase Heat Transfer* [19].

$$B(e^+) = \sqrt{\frac{2}{f}} + 2.5\ln\left(\frac{2e}{D}\right) + 3.75,$$ (10)

where f is the friction factor and e^+ is defined as

$$e^+ = \frac{e}{D}Re\sqrt{\frac{f}{2}}.$$ (11)

The following transcendental correlation provides the Stanton number.

7

$$g(e^+)\Pr^n = \frac{f/(2\,St) - 1}{\sqrt{f/2}} + B(e^+), \tag{12}$$

which when reduced results in the following relationship:

$$St = \frac{f/2}{1 + \sqrt{f/2}\left(g(e^+)\Pr^n - B(e^+)\right)}. \tag{13}$$

The ratio of the smooth Stanton number to that of the current "rough" Stanton number using the erosion depth as the dimension of the defect "e" provides some measure to the augmentation due to the flow disturbances of a sand grain type roughness.

5. Multicomponent Diffusion and Mass Transport Scheme

Mass transport to the surface is provided through a concentration potential $\phi_{i\,core\,flow} - \phi_{i\,wall}$ for each species i and a mass transport coefficient, h_m, derived from Sherwood number correlations integrated over space and time [8], as shown in equation 14:

$$Mass_i = \int \int h_m \left(\phi_{i\,core-flow} - \phi_{i\,wall} \right) dA\,dt. \tag{14}$$

Currently, species are assumed not to penetrate the surface, with the exception of carbon; however, the diffusion module is general enough to readily incorporate this possibility in the future.

In order to derive the mass transport coefficient, h_m, for a specific species from the Sherwood number, $Sh \equiv h_m L/D_{AB}$, where L is a length parameter, the diffusion coefficient, D_{12}, of species 1 into species 2 must be determined. The Lennard-Jones 6–12 model is used to model the binary diffusion [20].

$$D_{12} = \frac{0.0026280\sqrt{T^3(M_1 + M_2)/2M_1 M_2}}{P\sigma_{12}^2\,\Omega_{12}^{(1,1)}(T_{12})}, \tag{15}$$

where M_1, M_2 are the molecular weights of the binary species, T is the temperature, P is the pressure, σ_{12} is the collision diameter, and $\Omega_{12}^{(1,1)}$ is the collisional cross section integral obtained through table interpolation.

The binary diffusion provides the basis for the multicomponent diffusion coefficient. Each binary diffusion possibility for species i, j, is used and weighted vs. all other possibilities in the following mixture coefficient combinatory methodology of Wilke in Anderson [21].

$$D_{im} = \frac{1 - X_i}{\displaystyle\sum_{j \neq i} \frac{X_j}{D_{ij}}}, \tag{16}$$

thus enabling the calculation of the diffusion coefficient for a particular specie into a mixture of many species.

Utilizing the collisional cross sections and diameters for viscosity as well as the molecular weight, the following relationship derived from kinetic theory [20] is utilized to determine the viscosity and subsequently the mixture viscosity using Wilke's rule in Anderson [21].

$$\mu = 2.6693 \times 10^{-5} \frac{\sqrt{MT}}{\sigma_{12}^2 \Omega_{12_\mu}} \tag{17}$$

The Schmidt number, $Sc = \mu/\rho D_{AB}$, where ρ is the density and μ is the mixture viscosity, is used to determine which regime of mass transport is applicable. At moderate Schmidt numbers ($10 < Sc < 1000$), the thickness of the boundary layer is much greater than the thickness of the

viscous sublayer; utilizing the momentum integral method, Ruckenstein [22] derived the following Sherwood number:

$$Sh = \frac{0.0097\, Re^{\frac{9}{10}} Sc^{\frac{1}{2}} \left(1.10 + 0.44\, Sc^{-\frac{1}{3}} - 0.70\, Sc^{-\frac{1}{6}} \right)}{1 + 0.064\, Sc^{\frac{1}{2}} \left(1.10 + 0.44\, Sc^{-\frac{1}{3}} - 0.70\, Sc^{-\frac{1}{6}} \right)}.$$ (18)

For higher Schmidt numbers ($Sc > 1000$), the thickness of the boundary layer becomes the order of magnitude of the thin wall-layer and the following relationship is applicable [23]:

$$Sh = 0.0102\, Re^{\frac{9}{10}} Sc^{\frac{1}{3}}.$$ (19)

These expressions for the Sherwood number have been compared [23] with much experimental data and agree well within the Schmidt number regions specified.

6. Equilibrium Kinetics

Equilibrium chemical processes are considered to dominate whenever the characteristic time for a fluid element to traverse the flow field of interest is much longer than the characteristic time for chemical reactions to approach equilibrium. As the pressure and temperature increase, the molecular collision frequency and energy per collision increases, which leads to smaller characteristic chemical times, and chemical processes approach equilibrium.

The condition for chemical equilibrium may be stated as the minimization of the Gibbs Free Energy. For a mixture of N species (e.g., atoms or molecules), where the number of moles of species, i, is denoted n_i, the Gibbs Free Energy per mole of mixture is given in terms of the Gibbs Free Energy of the individual species, g_i, the internal energy, e, the temperature, T, the entropy, s, the total pressure, p, and the specific volume, v.

10

$$G = \sum_{i=1}^{N} n_i \, g_i = e - Ts + pv \qquad (20)$$

The equilibrium method employed in the present study is based on the fact that at equilibrium the total Gibbs energy of the system attains a minimum value. The problem is to find the set of n_i's that minimizes G for a specified energy and specific volume (e, V), subject to the constraints of material balances. The standard solution to this type of problem is based on the method of Lagrange's undetermined multipliers. First we must recognize that the total number of atoms of each element in the system is constant. A particular atomic species is denoted by the subscript k, and A_k is the total number of atomic masses of the k-th element in the system, as determined by the initial constitution of the system. Denoting the number of atoms of the k-th element present in each molecule of chemical species i by a_{ik}, then the material balance on each element k may be written (M used here is the number of elements),

$$\sum_{k=1}^{M} \lambda_k \left(\sum_{i=1}^{N} (n_i a_{ik} - A_k) \right) = 0 \quad (k = 1,2,...,M) \qquad (21)$$

after introducing Lagrange multipliers, λ_k, for each element. Then a new function, F, is formed by addition of the last equation to G. The function, F, is identical to G since the summation term is zero. However, $\dfrac{\partial F}{\partial n_i}$ and $\dfrac{\partial G}{\partial n_i}$ are different since F incorporates the constraints of the material balances. The minimum of both F and G occurs when these partial derivatives are zero.

$$F = G + \sum_{k=1}^{M} \lambda_k \left(\sum_{i=1}^{N} n_i a_{ik} - A_k \right) \qquad (22)$$

$$\left(\frac{\partial F}{\partial n_i} \right)_{e,V,n_i} = \left(\frac{\partial G}{\partial n_i} \right)_{e,V,n_i} + \sum_{k=1}^{M} \lambda_k a_{ik} = 0 \quad (\text{for } F_{min}) \ (i = 1, N) \qquad (23)$$

11

This equation can be rewritten using the definition of chemical potential α_i, for species i, where R_u is the universal gas constant.

$$\delta_i = \left(\frac{\partial G}{\partial n_i}\right)_{e, V, n_i} = G_i^o + R_u T \ln(\alpha_i) \quad (i = 1, N) \tag{24}$$

Therefore, from equation 23

$$\delta_i + \sum_{k=1}^{M} \lambda_k a_{ik} = 0 \quad (i = 1, 2, ..., N). \tag{25}$$

The standard Gibbs Free Energy change of formation for species i is denoted G_i^o, which is equal to zero for elements in their standard states. The activity for species i in solution is given by α_i defined in terms of the equilibrium constant, K, as,

$$K = \Pi_i^N \alpha_i^{v_i}, \tag{26}$$

where the activities of the components are raised to the corresponding stoichiometric coefficients, v_i. For an ideal gas mixture ($X_i \phi_i = 1$), where ϕ_i is the void fraction,

$$\alpha_i = f_i = X_i \phi_i p = p, \tag{27}$$

where f_i is the fugacity and X_i is the mole fraction for the i-th species. For liquid and solid phases [24],

$$\ln(\alpha_i) = \ln(1 - 1/p), \tag{28}$$

which is approximately zero for large pressure, therefore, $\delta_i = G_i^o$ from equation 24.

12

There are N equilibrium equations (equation 25), one for each species, and there are M material-balance equations (equation 21), one for each element, a total of N + M equations. The unknowns in these equations are the n_i's, of which there are N, and the λ_k's, of which there are M, a total of N + M. Thus, the number of equations is sufficient for the determination of all unknowns. Numerical experiments were performed with well-known gas-phase systems of which the results matched those of the NASA Lewis equilibrium code [14].

7. Surface Description

The full equilibrium control volume approach results in many product mass fractions, which are physically impossible due to the constraints of diffusion into the solid phase. Mainly, the carbon in the control volume, which results from CO and/or CO_2 breakdown, will react with as much iron as possible to form Fe_3C if permitted. To treat this deficiency, the carbon content in the steel resulting from the diffusion over the current time step has been integrated. This represents the total amount of carbon that may possibly react with the steel while the extra carbon released into the control volume is left as carbon graphite C(GR).

A surface exposed to a carbon concentration G per unit surface area for a specified length of time t has a carbon concentration C(x) at a specified depth of x given by the following relationship [25]:

$$C(x) = \frac{G}{\sqrt{\pi Dt}} e^{\frac{-x^2}{4Dt}}, \tag{29}$$

where D is the diffusion coefficient provided over the α and γ phases (BCC and FCC lattice structure, respectively). The diffusion of carbon into α iron (T < 1118° C) is given by the following function in *Smithells Metals Reference Handbook* [25], where R_u is the universal gas constant.

$$D = 0.008\,e^{\frac{-19.8\,(\text{cal/mol})}{R_u T}} + 2.2\,e^{\frac{-29.3\,(\text{cal/mol})}{R_u T}}\left(\frac{\text{cm}^2}{\text{s}}\right), \qquad (30)$$

while the diffusion of carbon into γ iron ($T < 1300°\,C$) is provided by

$$D = 0.36\,e^{\frac{36\,(\text{cal/mol})}{R_u T}}\left(\frac{\text{cm}^2}{\text{s}}\right). \qquad (31)$$

To find the total amount of carbon that has diffused in time t, the concentration function can be integrated, having an error function solution as

$$\int_0^x C(x)\,dx = \frac{G}{\sqrt{\pi D t}}\int_0^x e^{\frac{-x^2}{4Dt}}\,dx = G(\text{erf}(x)). \qquad (32)$$

Integrating the concentration profile to the maximum depth to which material can diffuse in time step t, $\sqrt{(Dt)}$, provides the carbon diffused into the material over the time period. Usually this depth ranges from 20 to 80 lattice parameters. To treat the reactant product from the full equilibrium calculation, a subset reaction is created consisting of the carbon, iron (α) and iron (γ), and iron carbide. The total carbon available for reaction is equal to the diffused carbon plus the original carbon in the steel as well as the possible carbon on surface, also in the form of iron carbide as shown on the left-hand side of the following equation:

$$C(GR) + Fe_3C + Fe(\alpha) + Fe(\gamma) \rightarrow C(GR) + Fe_3C + Fe(\alpha) + Fe(\gamma), \qquad (33)$$

where Fe(α) or Fe(γ) are supplied as fresh material, as needed, depending upon the control volume temperature. There is assumed no carbon dissolved in Fe(α) or Fe(γ). The product carbon C(GR), in the lattice, and Fe$_3$C from the previous time step are retained as residuals and reintroduced as reactants in the next time step. Carbon graphite is permitted to form or be simply transferred from a reactant to a product unchanged on the right-hand side if there is excess carbon from the

14

equilibrium calculation in comparison to what is possibly available to react with the existing iron. The amount of Fe_3C that is possible, due to diffusion limitations, is formed and carried over to the next time step if the control volume is below the melting temperature of the iron carbide. On the other hand, if there is no excess carbon, then $Fe(\alpha)$ or $Fe(\gamma)$, depending on the temperature, is formed or carried over to the next time step. Once this post equilibrium calculation is made, the final energy change in the control volume is recomputed and the amount attributable to the residual solids is accounted for as the surface source term.

8. Application to Point Studies

Three systems are presented in this report including the M829A2 cartridge in an M256 tank cannon and both the 616W-APFSDS original cartridge, which had a propellant adiabatic flame temperature near 3,650 K, and the M791-APDS-T training round in the 25-mm Bushmaster cannon.

The calculations for the M829A2 cartridge assume an initial chrome defect or chip. Two calculations were then performed for this region using exposed steel. The first involved normal or standard heat transfer, and the second applied the previously described surface irregularity augmentation to the heat transport due to the actual depth of the defect. The calculations were performed over a region from the forcing cone to about 800 mm down-bore.

Surface temperatures of the first calculation, without the surface roughness factor, are presented in Figure 2. As shown, all three locations reach the user-prescribed melting temperature of 1,723 K.

Figure 3 shows the amount of material lost over the investigated region in comparison to experimental data [26, 27] for three gun tubes. The experimental defect data show widely varying erosion once a defect is formed, with the average presented as a straight line. The tube history is provided as the number of rounds fired to the commencement of the series of M829A2 cartridges, the number of M829A2 cartridges fired, and the serial number of the tube.
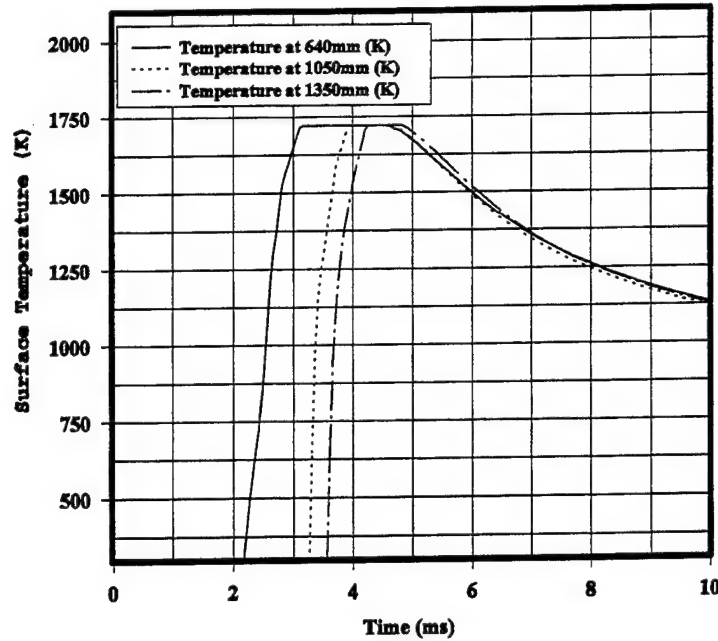
Figure 2. Gun Tube Surface Temperatures at Three Axial Locations for a Single Firing of an M829A2 Cartridge in an M256 Tank Cannon Without Surface Roughness Augmentation to the Heat Transport.

Figure 3. Average Erosion Depth per Round at the Bottom of a Chrome Chip in an M256 Tank Cannon Firing an M829A2 Cartridge Without Surface Roughness Augmentation to the Heat Transport.

16

Figure 4 shows the effect of added surface roughness to the calculation in lengthening the duration of the melting of the surface. Correspondingly, in Figure 5, the amount of erosion is shown to also increase. The resultant amount of erosion appears to be much closer to the average amount from the experimental "pit-tracking" data in Figure 5 with the augmentation than without it in Figure 3.
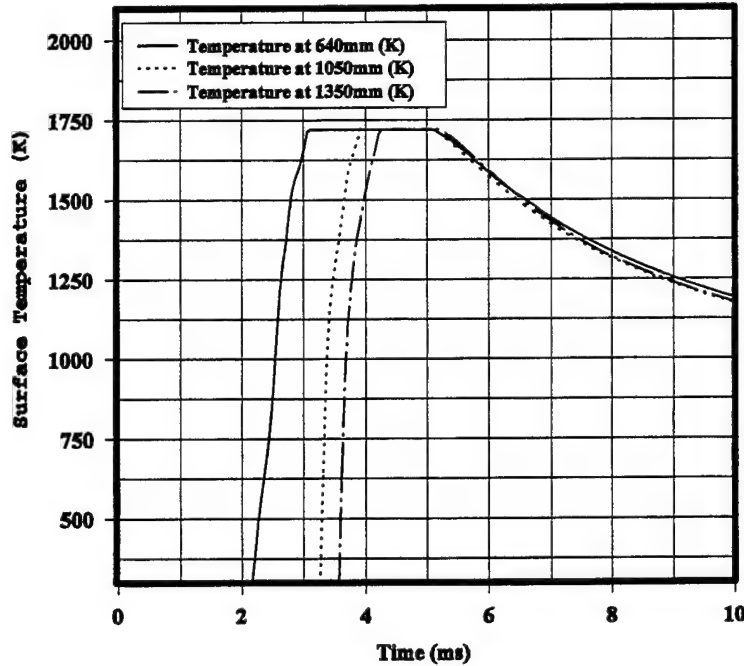
Figure 4. Gun Tube Surface Temperatures at Three Axial Locations and for a Single Firing of an M829A2 Cartridge in an M256 Tank Cannon With Surface Roughness Augmentation to the Heat Transport.

The total erosion in these calculations is due to the sum of the gross melting and the melting of iron carbide created near the surface due to the carbon diffusion. This effect can be seen in Figure 6 without, and in Figure 7 with, the surface roughness augmentation to the heat transport. Figure 6 shows the surface temperature, which does not rise to the melt temperature of the steel substrate. Material, however, is being removed at the surface due to the local surface material melt temperature of 1,423 K. The same figure presents how the change in phase from α to γ alters the diffusion rate due to different interstitial atomic mobilities.

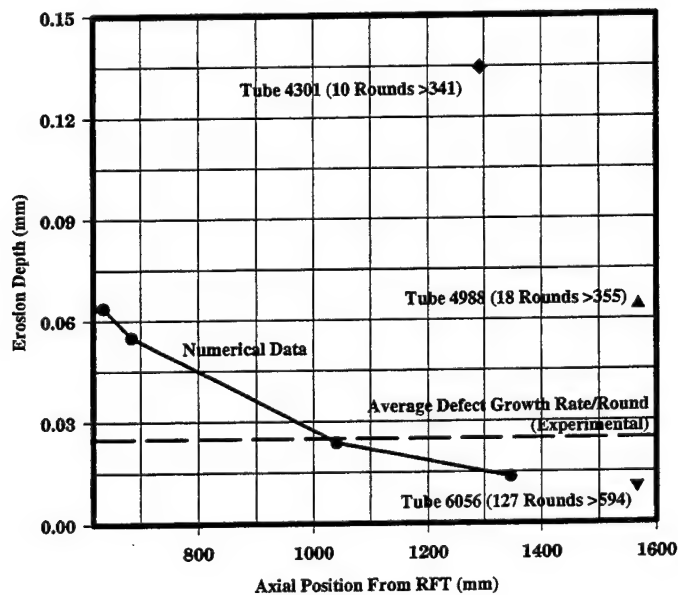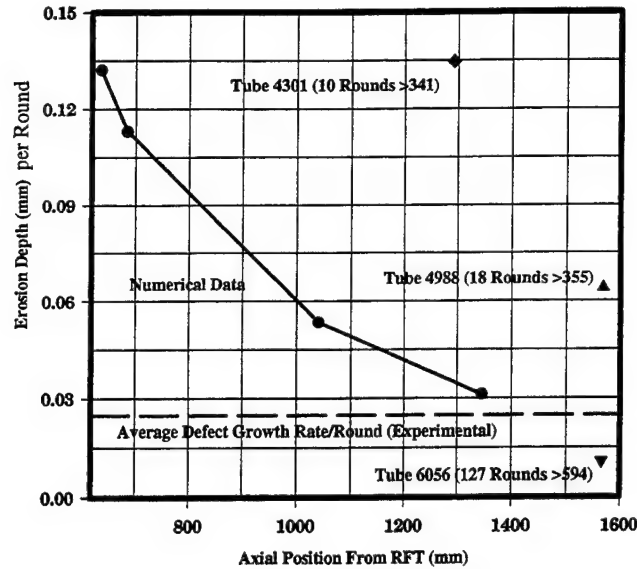Figure 5.   Average Erosion Depth per Round at the Bottom of a Chrome Chip for an M256 Cannon Firing an M829A2 Cartridge With Surface Roughness Augmentation to the Heat Transport.
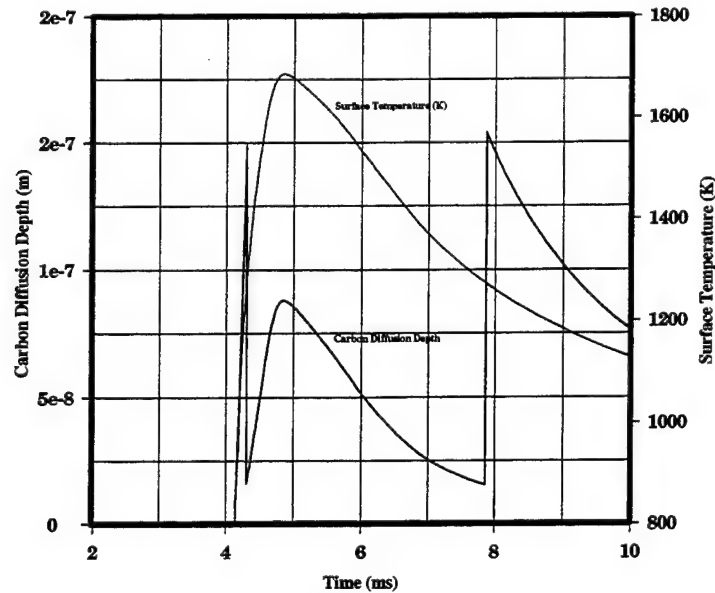
Figure 6.   Surface Temperature and Carbon Diffusion Depth at the Bottom of a Chrome Chip in an M256 Tank Cannon Firing an M829A2 Cartridge, Presented at 1,778 mm From the Rear Face of the Tube Without Surface Roughness Augmentation to the Heat Transport.

18
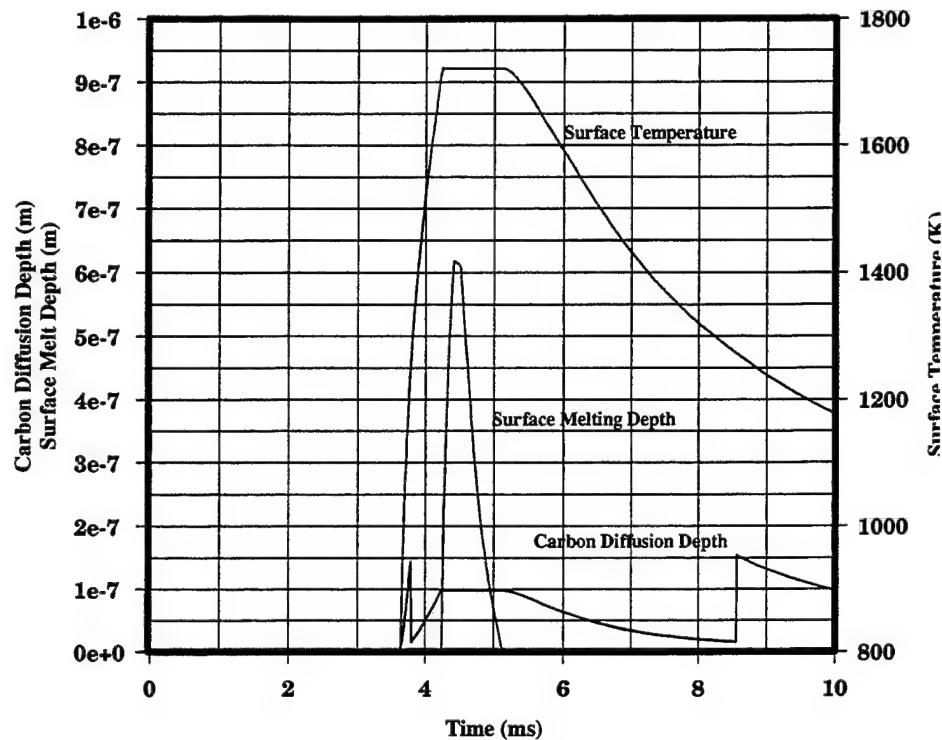
Figure 7. Surface Temperature, Carbon Diffusion Depth, and Surface Melting Depth in a Chrome Chip of an M256 Tank Cannon, Presented 1,350 mm From the Rear Face of the Tube for an M829A2 Cartridge With Surface Roughness Augmentation to the Heat Transport.

Figure 7 shows the influence of gross surface melting at the same axial location due to the addition of surface roughness augmentation. Once the surface reaches the base material melt temperature, the carbon diffusion remains constant, as it only depends upon temperature.

The first of the two 25-mm systems in this study is the M791 APDS-T round. Experimental data were obtained from a late 1980's study performed by Veritay Inc. [28] in their instrumented test fixture. The data included averaged erosion rate/round (over 20 individual rounds were averaged) at a series of axial locations given with respect to the commencement of full rifling. When the calculations were performed using the interior ballistic data provided by Benet Laboratories [29], the results were presented with respect to the rear face of the tube (RFT). This leads to a possible

discrepancy of the actual location of the origin of rifling as this location has a tendency to move down-bore as the tube has more rounds fired through it.

The surface temperatures of the cannon firing the M791 cartridge are shown in Figure 8. While these temperatures do not reach the bulk melting temperature of the steel used in the 25-mm nonchromed nitrided Bushmaster cannon of 1,792 K, there is material loss nonetheless. The nitriding was not taken into account in these calculations and would cause some differences in subsurface carbon diffusion. Again, as in the previous example, the material is being lost in this case due to the material transformation to iron carbide and the subsequent removal of this very thin layer when the surface temperature is above the melt temperature of the iron carbide.
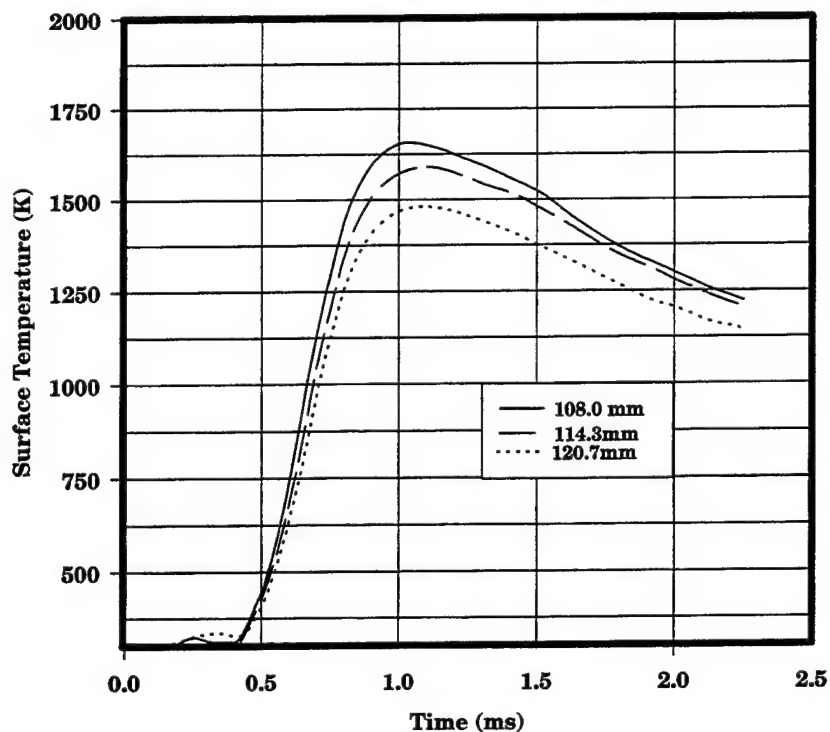
Figure 8. Surface Temperatures for Three Axial Locations of an M791 Cartridge Fired in an M242, 25-mm Bushmaster Cannon.

The result of the computed surface material removal for the M791 is presented in Figure 9 along with the experimental data and the location of full rifling. Although the axial location seems to be shifted as stated before, the magnitude of material loss appears to be correct. The surface roughness augmentation to the heat transfer was not used in this case as the surface is not chromed and therefore does not have the site for high recirculating flows.
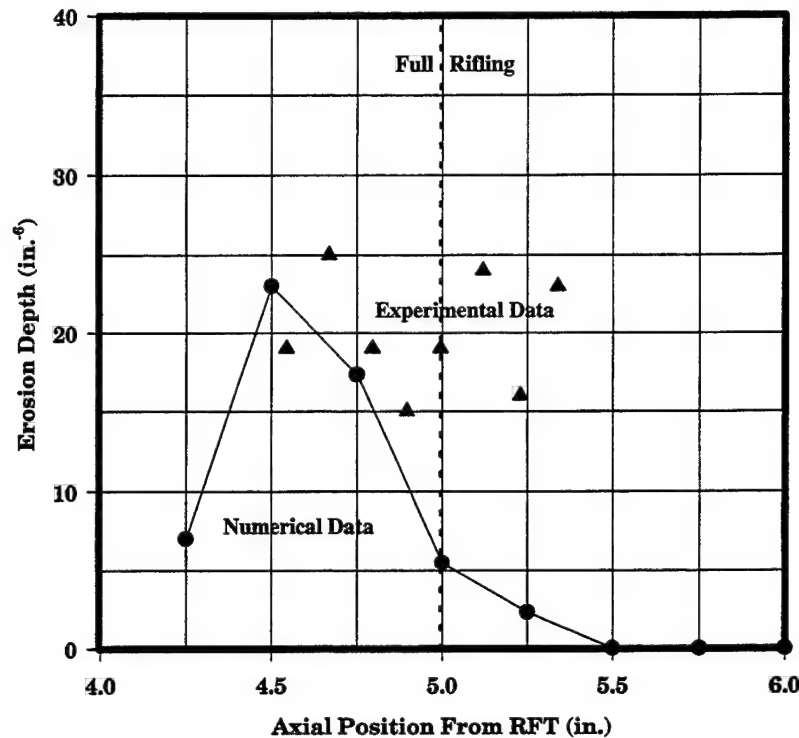
Figure 9. Computed and Experimental Erosion per Round for an M791 Cartridge Fired in a 25-mm Bushmaster Cannon. Note That the Experimental Data Were Originally Presented With Respect to the Commencement of "Full Rifling," While the Computational Data Are Presented With Respect to the RFT.

Figure 10 shows the bore surface temperatures for the cannon firing the 616W (M919 original) cartridge. Also, for this case, the melting temperature of the base material of the Bushmaster cannon is not reached. However, the temperatures are indeed somewhat higher in this case than for the M791 cartridge, and the surface material removed, shown in Figure 11, reflects the higher diffusion of carbon into the gun surface.

21
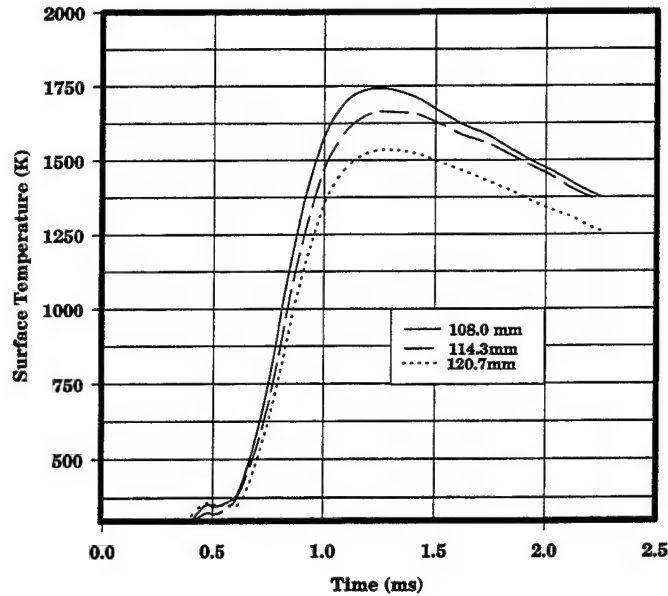
Figure 10. Surface Temperatures for Three Axial Locations for a 616W (Original M919 APFSDS) Cartridge Fired in an M242 Bushmaster Cannon.
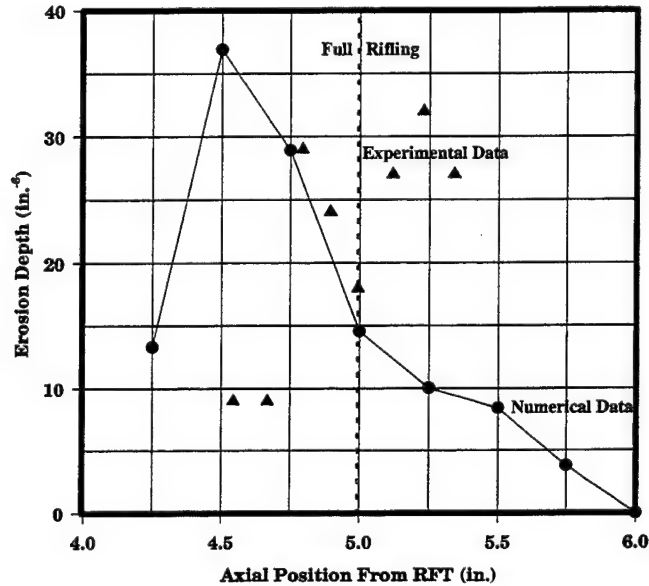
Figure 11. Computed and Experimental Erosion per Round for a 616W (Original M919 APFSDS) Cartridge Fired in an M242, 25-mm Bushmaster Cannon. Note That the Experimental Data Were Originally Presented With Respect to the Commencement of "Full Rifling," While the Computational Data Are Presented With Respect to the RFT.

22

The experimental data in Figure 11 again appears to be shifted with respect to the commencement of rifling, while the magnitude tracks the experimental data well. From Figures 11 and 9, it is shown that the proportional experimental increase in material loss between the M791 and 616W is closely represented in the numerical calculations.

9. Concluding Remarks

An analytical description of the processes involved in the mechanistic description of the gas-surface interaction has been presented to include the melt wipe mechanism, equilibrium chemistry, surface control volume, heat transfer and roughness augmentation, as well as the multicomponent mass transport, and subsurface carbon diffusion.

Three systems were investigated: the M829A2 120-mm tank cartridge, and two 25-mm cartridges: the M791-APDS-T and the 616W-APFSDS. The calculated erosion for the M829A2 cartridge, given the assumption of a chip in the chrome plating, compared well with the experimental data once the surface roughness was incorporated into the heat transport. Neither of the 25-mm systems reached the bulk melting temperature of the base material for the Bushmaster barrel, although both erode. Carbon diffusion limited erosion predicted the amount of material lost in the M791 and 616W cartridges reasonably well.

Other constitutive models and/or conceptual ideas and additional physics are to be investigated to determine their level of importance to surface degradation/erosion, thus providing insight into the mechanisms for erosion and possibly the mitigation thereof through additives to control the heat transfer, gas chemistry, or possibly altering the structure or physics of the surface.

INTENTIONALLY LEFT BLANK.

24

10. References

1. Ward, J. R., T. L. Brosseau, R. P. Kaste, I. C. Stobie, and B. Bensinger. "Erosivity of LOVA Propellants." BRL-TR-02368, U.S. Army Ballistic Research Laboratory, Aberdeen Proving Ground, MD, September 1981.

2. Caveny, L. H. "Steel Erosion Produced by Double Base, Triple Base, and RDX Composite Propellants of Various Flame Temperatures." ARLCD-CR-80016, U.S. Army Armament Research and Development Command, Picatinny Arsenal, NJ, October 1980.

3. Huang, P., M. Cole, and C. Hubbard. Personal communication. U.S. Army Research Laboratory, Aberdeen Proving Ground, MD, April 1998.

4. Montgomery, J. Personal communication. U.S. Army Research Laboratory, Aberdeen Proving Ground, MD, March 1998.

5. Evans, M. R. "User's Manual for Transient Boundary Layer Integral Matrix Procedure TBLIMP." Aerotherm UM-74-55, Prepared for Naval Ordnance Station, Indian Head, MD, October 1974.

6. Dunn, S., D. Coats, G. Nickerson, S. Sopok, P. O'Hara, and G. A. Pflegl. "Unified Computer Model for Predicting Thermochemical Erosion in Gun Barrels." AIAA 95-2440, *Proceedings of 31st AIAA/ASME/SAE/ASEE, San Diego, CA, Joint Propulsion Conference and Exhibit*, July 1995.

7. Weinacht, P., and P. J. Conroy. "A Numerical Method for Predicting Thermal Erosion in Gun Tubes." ARL-TR-1156, U.S. Army Research Laboratory, Aberdeen Proving Ground, MD, July 1996.

8. Conroy, P. J., P. Weinacht, and M. J. Nusca. "120-mm Gun Tube Erosion Including Surface Chemistry Effects." ARL-TR-152, U.S. Army Research Laboratory, Aberdeen Proving Ground, MD, 6 October 1997.

9. Gough, P. S. "The XNOVAKTC Code." BRL-CR-627, U.S. Army Ballistic Research Laboratory, Aberdeen Proving Ground, MD, February 1990.

10. Nusca, M. J. "Investigation of Solid Propellant Gun Systems Using the Next-Generation Interior Ballistics Code." *Proceedings of the 31st JANNAF Combustion Subcommittee Meeting*, CPIA Publication No. 620, vol. 1, pp. 279–292, October 1994.

11. Freedman, E. "BLAKE - A Thermodynamic Code Based on Tiger: Users' Guide and Manual." BRL-TR-02411, U.S. Army Ballistic Research Laboratory, Aberdeen Proving Ground, MD, July 1982.

12. Anderson, R. D., and K. D. Fickie. " IBHVG2 - A Users Guide." BRL-TR-2829, U.S. Army Ballistic Research Laboratory, Aberdeen Proving Ground, MD, July 1987.

13. Janke, P. J., J. A. Dyvik, and C. L. Marksberry. "Electrothermo-Chemical Propellant Extensions to the IBHVG2 Interior Ballistics Simulation: Model Development and Validation." CPIA Publication No. 620, vol. 3, pp. 171–181, October 1994.

14. Gordon, S., and B. J. McBride. "Computer Program for Calculation of Complex Chemical Equilibrium Compositions, Rocket Performance, Incident and Reflected Shocks, and Chapman-Jouget Detonations." NASA SP-273, NASA Lewis, Cleveland, OH, 1971.

15. Landau, H. G. "Heating Conduction in a Melting Solid." *Quarterly of Applied Mathematics*, vol. 8, pp. 81–94, 1950.

16. Stratford, B. S., and G. S. Beavers. "The Calculation of the Compressible Turbulent Boundary Layer in Arbitrary Pressure Gradient - A Correlation of Certain Previous Methods." Aeronautical Research Council, Royal Armament Research and Development Establishment, Seven Oaks, United Kingdom, R&M, No. 3207, 1961.

17. Conroy, P. J. "Gun Tube Heating." BRL-TR-3300, U. S. Army Ballistic Research Laboratory, Aberdeen Proving Ground, MD, December 1991.

18. Miller, R. *Flow Measurement Handbook*, New York: McGraw-Hill Publishing, 1989.

19. Kakac, S., R. K. Shah, and W. Aung. *Handbook of Single-Phase Heat Transfer*. New York: John Wiley and Sons Inc., 1987.

20. Hirschfelder, J. O, C. F. Curtis, and R. B. Bird. *Molecular Theory of Gases and Liquids*. New York: John Wiley and Sons Inc., March 1964.

21. Anderson, J. D. *Hypersonic + High Temperature Gas Dynamics*. New York: McGraw-Hill, 1989.

22. Ruckenstein, E. "Some Remarks on Renewal Models." *Chemical Engineering Science*, vol. 18, p. 223, 1963.

23. Gutfinger, C. *Topics in Transport Phenomena*. New York: John Wiley and Sons, 1975.

24. Smith, J. M., and H. C. Van Ness. *Introduction to Chemical Engineering Thermodynamics*. New York: McGraw-Hill Book Company, Fourth Edition, p. 516, 1987.

25. Brandes, E. A. *Smithells Metals Reference Handbook, Sixth Edition*. Boston, MA: Butterworth & Co., 1983.

26. Hubbard, C., and R. Gilley. Bore Scope Records. U. S. Army Aberdeen Test Center, Aberdeen Proving Ground, MD, 1998.

27. U.S. Department of the Army. *Evaluation of Cannon Tubes.* TM 9-1000-202-14, 1 March 1992.

28. Talley, J. Q., and J. A. Owczarczak. "25-mm Barrel Erosivity Study." Final Report Prepared for GenCorp Aerojet Corporation, Aerojet Ordnance Division, Downey, CA, August 1991.

29. O'Hara, G. P. Personal communication of 25-mm interior ballistic data decks. Benet Laboratories, Watervliet Arsenal, Watervliet, NY, July 1997.

INTENTIONALLY LEFT BLANK.

Appendix A:

Blake Thermochemical Input Decks for Propellants Used in This Study

INTENTIONALLY LEFT BLANK.

Blake Thermochemical input deck for the 25-mm M791 Cartridge using HC-33 propellant.

```
TIT,HC-33 NOM
ING
PRL,CON,2
REJ,H2S,S2O,SO2,K$,KOH$,K2O,K2O2,KO2,K2,NO2,HNO3
REJ,KCO$,KSO$,K2O$,NA2$,ALN,COF2,F2,ALF3,ALO,ALF2,AL23,AL$
REJ,C2N,C2H,C2,CH2O,CH,CH2,CH3,CN,C2H2,C2H4,C2N2,
REJ,ALOH,A2O2,AHO2,ALOF,AIO2,BAO$
REJ,C(S),K2CO3$,K2SO4$,K2S$
CM2,NC1325,87.87,NG,6.99,PEG,.68,KN,.66,ALC,.5,ACETON,1.4,H2O,.9,C,.15,
DPA,0.85
UNI,ENG
GUN,.05,.05,.6
QUIT
```

Blake Thermochemical input decks for the Original 25-mm M919 Cartridge.

```
TIT,HES9053 (L-751) Propellant
ING
PRL,CON,2
REJ,H2S,S2O,SO2,K$,KOH$,K2O,K2O2,KO2,K2,NO2,HNO3
REJ,KCO$,KSO$,K2O$,NA2$,ALN,COF2,F2,ALF3,ALO,ALF2,AL23,AL$
REJ,C2N,C2H,C2,CH2O,CH,CH2,CH3,CN,C2H2,C2H4,C2N2,
REJ,ALOH,A2O2,AHO2,ALOF,AIO2,BAO$
REJ,C(S),K2CO3$,K2SO4$,K2S$
CM2,NC1300,34.40,NG,14.91,RDX,45.60,TRIAC,2.90,PEG,0.31,EC,0.52,KN,0.75,
KS,0.75,H2O,.10,C,0.20
UNI,ENG
GUN,.05,.05,.6
QUIT
```

```
TIT,HES9053 (L-752) Propellant
ING
PRL,CON,2
REJ,H2S,S2O,SO2,K$,KOH$,K2O,K2O2,KO2,K2,NO2,HNO3
REJ,KCO$,KSO$,K2O$,NA2$,ALN,COF2,F2,ALF3,ALO,ALF2,AL23,AL$
REJ,C2N,C2H,C2,CH2O,CH,CH2,CH3,CN,C2H2,C2H4,C2N2,
REJ,ALOH,A2O2,AHO2,ALOF,AIO2,BAO$
REJ,C(S),K2CO3$,K2SO4$,K2S$
CM2,NC1300,35.38,NG,14.71,RDX,43.48,TRIAC,3.04,PEG,1.36,EC,0.52,KN,0.84,
KS,0.77,H2O,.23,C,0.20
UNI,ENG
GUN,.05,.05,.4
QUIT
```

```
TIT,HES9053 (L-753) Propellant
ING
PRL,CON,2
REJ,H2S,S2O,SO2,K$,KOH$,K2O,K2O2,KO2,K2,NO2,HNO3
REJ,KCO$,KSO$,K2O$,NA2$,ALN,COF2,F2,ALF3,ALO,ALF2,AL23,AL$
REJ,C2N,C2H,C2,CH2O,CH,CH2,CH3,CN,C2H2,C2H4,C2N2,
REJ,ALOH,A2O2,AHO2,ALOF,AIO2,BAO$
REJ,C(S),K2CO3$,K2SO4$,K2S$
CM2,NC1300,35.71,NG,12.73,RDX,44.78,TRIAC,3.24,PEG,1.08,EC,0.63,KS,1.05,
KN,0.78,H2O,.24,C,0.020
UNI,ENG
GUN,.05,.05,.4
QUIT
```

```
TIT,HES9053 (L-754) Propellant
ING
PRL,CON,2
REJ,H2S,S2O,SO2,K$,KOH$,K2O,K2O2,KO2,K2,NO2,HNO3
REJ,KCO$,KSO$,K2O$,NA2$,ALN,COF2,F2,ALF3,ALO,ALF2,AL23,AL$
REJ,C2N,C2H,C2,CH2O,CH,CH2,CH3,CN,C2H2,C2H4,C2N2,
REJ,ALOH,A2O2,AHO2,ALOF,AIO2,BAO$
REJ,C(S),K2CO3$,K2SO4$,K2S$
CM2,NC1300,32.25,NG,14.94,RDX,47.73,TRIAC,2.75,PEG,0.35,EC,0.45,KS,0.78,
KN,0.75,H2O,.23,C,0.20
UNI,ENG
GUN,.05,.05,.4
QUIT
```

Blake Thermochemical input deck for 120-mm Cartridges using nominal JA2 propellant.

```
TIT,JA-2 - NOMINAL
PRL,CON,2
REJ,H2S,S2O,SO2,K$,KOH$,K2O,K2O2,KO2,K2,NO2,HNO3
```

```
REJ,KCO$,KSO$,K2O$,NA2$,ALN,COF2,F2,ALF3,ALO,ALF2,AL23,AL$
REJ,C2N,C2H,C2,CH2O,CH,CH2,CH3,CN,C2H2,C2H4,C2N2,
REJ,ALOH,A2O2,AHO2,ALOF,AIO2,BAO$
REJ,C(S),K2CO3$,K2SO4$,K2S$
CM2,NC1298,59.02,NG,14.78,DEGDN,24.60,AKAR2,.69,BAO,0.0496,
C,.0496,H2O,.5
UNI,ENG
GUN,.05,.05,.4
QUIT
```

Appendix B:

XKTC Interior Ballistic Input Decks
Used in This Study

INTENTIONALLY LEFT BLANK.

An XKTC input deck of an M829A2 round (Courtesy of Dr. G. Peter O'Hara, Benet Labs)

```
M829A2 APFSDS-T
TTFFTTT0010000010600000010010000000
    69   -3    099999          .0001
     0.015    186.660   0.00025      2.000      0.050      0.005     0.0001     0.0001
  1000   100 1100   100 1500   100
     6     4     3     4     0     0     3     2     0     0     0     8     0     0     0     1
     0     0     0
  5.290E+02 1.470E+01 2.890E+01 1.400E+00 0.000E+00 0.000E+00 0.000E+00 0.000E+00
  5.290E+02 0.000E+00 0.000E+00 0.000E+00 0.000E+00 0.000E+00 0.000E+00
   Stick              0.000E+00 7.500E-01 4.400E-01 5.763E-02 0.000E+00 0.000E+00
  1.925E+01 2.200E+01 8.600E-01 0.000E+00 0.000E+00
       7 4.310E-01 3.100E-02 8.750E-01 7.000E+00 0.000E+00     0 0.000E+00     0
  1.000E+04 1.000E+00 4.175E+04 0.000E+00 5.000E-01
  1.000E+04 4.040E-03 7.162E-01 1.000E+05 8.600E-04 8.796E-01 0.000E+00 8.000E+02
  2.770E-02 1.345E-04 6.000E-01
  2.037E+07 2.482E+01 1.227E+00 2.698E+01
   Stick              7.500E-01 1.925E+01 1.490E+00 5.763E-02 0.000E+00 0.000E+00
       7 3.840E-01 3.900E-02 5.980E-01 7.000E+00 0.000E+00     0 0.000E+00     0
  1.000E+04 1.000E+00 4.175E+04 0.000E+00 5.000E-01
  1.000E+04 4.040E-03 7.162E-01 1.000E+05 8.600E-04 8.796E-01 0.000E+00 8.000E+02
  2.770E-02 1.345E-04 6.000E-01
  2.037E+07 2.482E+01 1.227E+00 2.698E+01
   JA2H -             7.500E-01 1.925E+01 1.600E+01 5.763E-02 0.000E+00 0.000E+00
      15 6.710E-01 3.700E-02 8.750E-01 1.900E+01 0.000E+00     0 0.000E+00     0
  1.000E+04 1.000E+00 4.175E+04 0.000E+00 5.000E-01
  1.000E+04 4.040E-03 7.162E-01 1.000E+05 8.600E-04 8.796E-01 0.000E+00 8.000E+02
  2.770E-02 1.345E-04 6.000E-01
  2.037E+07 2.482E+01 1.227E+00 2.698E+01
  9.968E+06 3.093E+01 1.221E+00 2.300E+01
  0.000E+00 2.500E-04 1.250E-03 1.500E-03
  5.000E-01 4.800E+00 4.810E+00
  0.000E+00 0.000E+00 0.000E+00
  1.400E+01 1.400E+01 0.000E+00
  1.400E+01 1.400E+01 0.000E+00
  0.000E+00 0.000E+00 0.000E+00
  0.000E+00 2.250E+00 3.000E+00 3.090E+00 1.900E+01 3.090E+00 2.200E+01 2.380E+00
  2.373E+01 2.360E+00 2.087E+02 2.360E+00
  0.000E+00 1.000E+02 1.000E+00 1.500E+03 1.500E+00 4.000E+02 2.500E+02 4.000E+02
  1.400E+00 1.470E+01 5.290E+02 2.890E+01
  5.000E-02 4.850E-01 6.000E+00 2.000E+00
  7.770E+00 2.280E-02 7.000E-01
  0.000E+00 1.000E+01 0.000E+00 1.000E+00 1.000E+00
  2.200E+01 1.720E+01 4.400E+01 0.000E+00 0.000E+00 4.057E+03
        3.0      19.      30.      41.      60.      90.     120.      19.

     7     2     0     0     0     0     0     1     0     0     0     0     0     0
  0.000E+00 0.000E+00 7.200E-01 5.930E-01 4.380E+00 5.930E-01 4.880E+00 7.300E-01
  6.750E+00 7.300E-01 1.196E+01 1.170E+00 1.546E+01 1.420E+00
     3     4     0     0
  0.000E+00 1.450E-01 1.800E+01 1.450E-01 2.220E+01 5.000E-03
  2.950E-02 1.470E+01 4.550E-02 1.100E+04 4.970E-02 2.500E+04 5.480E-02 1.000E+05
     2     0     0
  1.000E+04 1.310E-04 1.301E+00 1.000E+05 3.950E+00 1.761E-01
  0.000E+00 8.000E+02 2.770E-02 1.345E-04 0.000E+00
  9.300E+06 2.239E+01 1.258E+00
```

An XKTC input deck of an M791 round (Courtesy of Dr. G. Peter O'Hara, Benet Labs)

```
  25MM M242           M791 - 135 gm       RESISTANCE-PERRIN
TTFFTTT00100000101010001000000000
    75   -2    099999    0    0    0.00001
       0.003    73.400    0.0002      1.500      0.050      0.01      0.0001      0.0001
  1000    50 1100    50
    10    3    3    10    2    0    1    1    0    0    0    5    0    0    0    0
     0    0    0
  5.300E+02 1.470E+01 2.890E+01 1.400E+00 0.000E+00 0.000E+00 0.000E+00 0.000E+00
  5.300E+02 0.000E+00 0.000E+00 0.000E+00 0.000E+00 0.000E+00 0.000E+00
  7 Perf HC33          7.300E-02 4.447E+00 2.141E-01 5.560E-02 0.000E+00 0.000E+00
     7 1.040E-01 1.000E-02 1.100E-01 7.000E+00 0.000E+00      0 0.000E+00      0
  1.740E+03 1.000E+00 5.000E+04 0.000E+00 5.000E-01
  4.000E+03 1.390E-03 8.053E-01 0.000E+00 5.300E+02 2.770E-02 1.345E-04 6.000E-01
  1.837E+07 2.511E+01 1.234E+00 2.801E+01
  1.837E+07 1.837E+07 9.500E-01 1.000E+00 2.370E-03
  9.968E+06 3.093E+01 1.221E+00 4.348E-02
  0.000E+00 1.200E-04 2.500E-04
  7.300E-02 2.730E-01 1.073E+00
  0.000E+00 0.000E+00 0.000E+00
  0.000E+00 3.000E+00 1.000E+00
  0.000E+00 0.000E+00 0.000E+00
  0.000E+00 2.500E-01 7.300E-02 2.875E-01 1.450E-01 4.865E-01 2.800E-01 5.800E-01
  5.530E-01 6.615E-01 8.330E-01 6.735E-01 3.876E+00 6.715E-01 4.447E+00 4.815E-01
  4.983E+00 5.040E-01 7.886E+01 5.040E-01
  0.000E+00 2.500E+03 3.600E-02 3.519E+03 9.600E-02 4.738E+03 2.040E-01 4.738E+03
  7.480E-01 2.126E+03 2.190E+00 1.220E+03 5.096E+00 8.520E+02 1.109E+01 7.360E+02
  2.941E+01 5.640E+02 9.000E+01 5.640E+02
  7.847E+00 2.280E-02 7.000E-01
  0.000E+00 5.300E+02 7.777E+01 5.300E+02
  0.000E+00 1.000E+00 1.000E+00 0.000E+00 1.000E+00
  4.700E+00 2.977E-01 1.000E-02 6.000E+00 0.000E+00 0.000E+00
       0.00      4.25      4.5      4.75      5.00
       0.07      0.00      0.00    2    0
    0    0    0    0    0    0    0    0    0    0    0    0    0    0
```

36

An XKTC input deck of an "original" M919 round (Courtesy of Dr. G. Peter O'Hara, Benet Labs)

```
  25MM M242           M919 Round - 132 gm RESISTANCE-PERRIN
TTFFTTT0010000010401000100000000000
    7099999      099999    0     0   0.00001
       .005     74.105   0.00002     1.500      0.050      0.003      0.0001      0.0001
    10    3     3    10     2     0     1     2     0     0     0     5     0     0     0     0
     0     0     0
5.300E+02 1.470E+01 2.890E+01 1.400E+00 0.000E+00 0.000E+00 0.000E+00 0.000E+00
5.300E+02 0.000E+00 0.000E+00 0.000E+00 0.000E+00 0.000E+00 0.000E+00
94.5 gm - HES-9053  7.300E-02 4.647E+00 2.083E-01 6.033E-02 0.000E+00 0.000E+00
    7 1.300E-01 1.250E-02 1.375E-01 7.000E+00 0.000E+00     0 0.000E+00     0
1.740E+03 1.000E+00 5.000E+04 0.000E+00 5.000E-01
4.000E+03 1.633E-04 1.179E+00 5.000E+03 5.077E-03 6.998E-01 0.000E+00 8.020E+02
2.770E-02 1.345E-04 6.000E-01
2.028E+07 2.498E+01 1.232E+00 2.847E+01
1.927E+07 2.028E+07 9.000E-01 1.000E+00 2.370E-03
9.968E+06 3.093E+01 1.221E+00 4.348E-02
0.000E+00 1.200E-04 2.500E-04
8.730E-01 1.073E+00 1.873E+00
0.000E+00 0.000E+00 0.000E+00
0.000E+00 3.000E+00 1.000E+00
0.000E+00 0.000E+00 0.000E+00
0.000E+00 2.500E-01 7.300E-02 2.875E-01 1.450E-01 4.865E-01 2.800E-01 5.800E-01
5.530E-01 6.615E-01 8.330E-01 6.735E-01 3.876E+00 6.735E-01 4.447E+00 4.815E-01
4.983E+00 5.040E-01 7.886E+01 5.040E-01
0.000E+00 2.500E+03 3.600E-02 3.519E+03 9.600E-02 4.738E+03 2.040E-01 4.738E+03
7.480E-01 2.126E+03 2.190E+00 1.220E+03 5.096E+00 8.520E+02 1.109E+01 7.360E+02
2.941E+01 5.640E+02 9.000E+01 5.640E+02
1.400E+00 1.470E+01 5.300E+02 2.890E+01
7.847E+00 2.280E-02 7.000E-01
0.000E+00 5.300E+02 7.886E+01 5.300E+02
2.500E+01 7.600E+01 0.000E+00 0.000E+00 1.000E+00
4.753E+00 2.913E-01 1.000E-02 6.000E+00 0.000E+00 0.000E+00
       0.00       4.00       4.25       4.5       4.75       5.00
```

INTENTIONALLY LEFT BLANK.

NO. OF
COPIES ORGANIZATION

2 DEFENSE TECHNICAL
INFORMATION CENTER
DTIC DDA
8725 JOHN J KINGMAN RD
STE 0944
FT BELVOIR VA 22060-6218

1 HQDA
DAMO FDQ
D SCHMIDT
400 ARMY PENTAGON
WASHINGTON DC 20310-0460

1 OSD
OUSD(A&T)/ODDDR&E(R)
R J TREW
THE PENTAGON
WASHINGTON DC 20301-7100

1 DPTY CG FOR RDA
US ARMY MATERIEL CMD
AMCRDA
5001 EISENHOWER AVE
ALEXANDRIA VA 22333-0001

1 INST FOR ADVNCD TCHNLGY
THE UNIV OF TEXAS AT AUSTIN
PO BOX 202797
AUSTIN TX 78720-2797

1 DARPA
B KASPAR
3701 N FAIRFAX DR
ARLINGTON VA 22203-1714

1 NAVAL SURFACE WARFARE CTR
CODE B07 J PENNELLA
17320 DAHLGREN RD
BLDG 1470 RM 1101
DAHLGREN VA 22448-5100

1 US MILITARY ACADEMY
MATH SCI CTR OF EXCELLENCE
DEPT OF MATHEMATICAL SCI
MADN MATH
THAYER HALL
WEST POINT NY 10996-1786

NO. OF
COPIES ORGANIZATION

1 DIRECTOR
US ARMY RESEARCH LAB
AMSRL DD
J J ROCCHIO
2800 POWDER MILL RD
ADELPHI MD 20783-1197

1 DIRECTOR
US ARMY RESEARCH LAB
AMSRL CS AS (RECORDS MGMT)
2800 POWDER MILL RD
ADELPHI MD 20783-1145

3 DIRECTOR
US ARMY RESEARCH LAB
AMSRL CI LL
2800 POWDER MILL RD
ADELPHI MD 20783-1145

ABERDEEN PROVING GROUND

4 DIR USARL
AMSRL CI LP (BLDG 305)

39

1	HQDA DIR R&D SAAL TR W MORRISON SUITE 9800 2511 JEFFERSON DAVIS HWY ARLINGTON VA 22201
1	HQS US ARMY MATERIEL CMD AMCICP AD 5001 EISENHOWER AVE ALEXANDRIA VA 22331-0001
1	US ARMY BMDS CMD ADVANCED TECHLGY CTR PO BOX 1500 HUNTSVILLE AL 35807-3801
1	OFC OF THE PRODUCT MGR SFAE AR HIP IP R DE KLEINE 155MM HOWITZER M109A6 PALADIN PICATINNY ARSENAL NJ 07806-5000
1	PM CRUSADER MUNITIONS SFAE GCSS CRM LTC D ARMOUR BLDG 171A PICATINNY ARSENAL NJ 07806-5000
1	CDR US ARMY ARDEC PROD BASE MODRNZTN AGENCY AMSMC PBM A SIKLOSI PICATINNY ARSENAL NJ 07806-5000
1	CDR US ARMY ARDEC PROD BASE MODRNZTN AGENCY AMSTA AR WES L LAIBSON PICATINNY ARSENAL NJ 07806-5000
1	PM PEO ARMAMENTS TANK MAIN ARMAMENT SYS AMCPM TMA PICATINNY ARSENAL NJ 07806-5000

1	PM PEO ARMAMENTS TANK MAIN ARMAMENT SYS AMCPM TMA 105 PICATINNY ARSENAL NJ 07806-5000
1	PM PEO ARMAMENTS TANK MAIN ARMAMENT SYS AMCPM TMA AS H YUEN PICATINNY ARSENAL NJ 07806-5000
2	CDR US ARMY ARDEC AMSTA AR CCH B C MANDALA E FENNELL PICATINNY ARSENAL NJ 07806-5000
1	CDR US ARMY ARDEC AMSTA AR CCS PICATINNY ARSENAL NJ 07806-5000
1	CDR US ARMY ARDEC AMSTA AR WE D DOWNS PICATINNY ARSENAL NJ 07806-5000
10	CDR US ARMY ARDEC AMSTA AR WEE M PADUANO S EINSTEIN S WESTLEY S BERNSTEIN J RUTKOWSKI B BRODMAN P O'REILLY R CIRINCIONE P HUI J O'REILLY PICATINNY ARSENAL NJ 07806-5000
3	CDR US ARMY ARDEC AMSTA AR AEE WW M MEZGER D WIEGAND P LU PICATINNY ARSENAL NJ 07806-5000

1   OFFICE OF NAVAL RSRCH
    CODE 473 J GOLDWASSER
    800 N QUINCY ST
    ARLINGTON VA 22217-9999

1   OFFICE OF NAVAL TECHLGY
    ONT 213 D SIEGEL
    800 N QUINCY ST
    ARLINGTON VA 22217-5000

6   CDR NAVAL SURFACE WARFARE
    CTR
    T C SMITH
    S MITCHELL
    S PETERS
    J CONSAGA
    C GOTZMER
    TECH LIB
    INDIAN HEAD MD 20640-5000

1   CDR NAVAL SURFACE WARFARE
    CTR
    CODE G30 GUNS & MUNITIONS DIV
    DAHLGREN VA 22448-5000

1   CDR NAVAL SURFACE WARFARE
    CTR
    CODE G32
    GUNS SYSTEMS DIV
    DAHLGREN VA 22448-5000

1   CDR NAVAL SURFACE WARFARE
    CTR
    CODE E23
    TECH LIB
    DAHLGREN VA 22448-5000

2   CDR NAVAL AIR WARFARE CTR
    CODE 388
    C F PRICE
    T BOGGS
    CHINA LAKE CA 93555-6001

2   CDR NAVAL AIR WARFARE CTR
    CODE 3895
    T PARR
    R DERR
    CHINA LAKE CA 93555-6001

1   CDR NAVAL AIR WARFARE CTR
    INFORMATION SCIENCE DIV
    CHINA LAKE CA 93555-6001

1   WL MNME
    ENERGETIC MATERIALS BR
    2306 PERIMETER RD
    STE 9
    EGLIN AFB FL 32542-5910

1   SDIO DA
    E GERRY
    PENTAGON
    WASHINGTON DC 21301-7100

2   HQ DTRA
    D LEWIS
    A FAHEY
    6801 TELEGRAPH RD
    ALEXANDRIA VA 22310-3398

1   DIR SANDIA NATL LABS
    M BAER DEPT 1512
    PO BOX 5800
    ALBUQUERQUE NM 87185

1   DIR SANDIA NATL LABS
    R CARLING
    COMBUSTION RSRCH FACILITY
    LIVERMORE CA 94551-0469

2   DIR LLNL
    L 355
    A BUCHINGHAM
    M FINGER
    PO BOX 808
    LIVERMORE CA 94550-0622

2   BATTELLE
    TWSTIAC
    V LEVIN
    505 KING AVE
    COLUMBUS OH 43201-2693

1   BATELLE PNL
    M GARNICH
    PO BOX 999
    RICHLAND WA 99352

1	CPI JHU H J HOFFMAN 10630 LITTLE PATUXENT PKWY STE 202 COLUMBIA MD 21044-3200
1	AFELM THE RAND CORP LIBRARY D 1700 MAIN ST SANTA MONICA CA 90401-3297
1	BRIGHAM YOUNG UNIV M BECKSTEAD DEPT OF CHEMICAL ENGRG PROVO UT 84601
1	CALIF INSTITUTE OF TECHLGY F E C CULICK 204 KARMAN LAB MAIN STOP 301 46 1201 E CALIFORNIA STR PASADENA CA 91109
1	MILLERSVILLE UNIV PHYSICS DEPT C W PRICE MILLERSVILLE PA 17551
2	UNIV OF ILLINOIS DEPT OF MECH INDUSTRY ENGRG H KRIER R BEDDINI 144 MEB 1206 N GREEN ST URBANA IL 61801-2978
1	UNIV OF MASSACHUSETTS DEPT OF MECHANICAL ENGRG K JAKUS AMHERST MA 01002-0014
1	UNIV OF MINNESOTA DEPT OF MECHANICAL ENERG E FLETCHER MINNEAPOLIS MN 55414-3368
4	PENNSYLVANIA STATE UNIV DEPT OF MECHANICAL ENGRG V YANG K KUO S THYNELL G SETTLES UNIVERSITY PARK PA 16802-7501

1	RUTGERS UNIVERSITY DEPT OF MECH AND AERO ENGRG S TEMKIN UNIV HEIGHTS CAMPUS NEW BRUNSWICK NJ 08903
1	UNIV OF UTAH DEPT OF CHEMICAL ENGRG A BAER SALT LAKE CITY UT 84112-1194
1	ARROW TECHLGY ASSOC INC 1233 SHELBURNE RD D-8 SOUTH BURLINGTON VT 05403
1	AAI CORPORATION D CLEVELAND PO BOX 126 HUNT VALLEY MD 21030-0126
7	ALLIANT TECHSYSTEMS INC R E TOMPKINS J BODE C CANDLAND L OSGOOD R BURETTA R BECKER M SWENSON 600 SECOND ST NE HOPKINS MN 55343
1	ELI FREEDMAN AND ASSOC E FREEDMAN 2411 DIANA RD BALTIMORE MD 21209-1525
6	ALLIANT TECHSYSTEMS INC L GIZZI D A WORRELL W J WORRELL C CHANDLER S RITCHIE A ZEIGLER RADFORD ARMY AMMO PLANT RADFORD VA 24141-0299
2	ALLIANT TECHSYSTEMS INC W B WALKUP T F FARABAUGH ALLEGHENY BALLISTICS LAB PO BOX 210 ROCKET CENTER WV 26726

43

NO. OF
COPIES ORGANIZATION

1	ALLIANT TECHSYSTEMS INC R CARTWRIGHT AEROSPACE 100 HOWARD BLVD KENVILLE NJ 07847		1	SOUTHWEST RSRCH INST J P RIEGEL 6220 CULEBRA RD PO DRAWER 28510 SAN ANTONIO TX 78228-0510
1	L MARTIN ARM SYS J TALLEY RM 1309 LAKESIDE AVE BURLINGTON VT 05401		1	KELLER SERVICES GEORGE KELLER 3510 GARRETT COURT ABERDEEN MD 21001-1232
1	PRIMEX F E WOLF BADGER ARMY AMMO PLANT BARABOO WI 53913		3	VERITAY TECHGY INC E FISHER R SALIZONI J BARNES 4845 MILLERSPORT HWY EAST AMHERST NY 14501-0305
3	PRIMEX E J KIRSCHKE A F GONZALEZ J DRUMMOND D W WORTHINGTON PO BOX 222 SAINT MARKS FL 32355-0222		1	PRIMEX E STEINER DIR LARGE CAL R & D PO BOX 127 RED LION PA 17356
2	PRIMEX N HYLTON J BUZZETT 10101 9TH ST NORTH ST PETERSBURG FL 33716		1	SRI INTERNATIONAL TECH LIB PROPULSION SCIENCES DIV 333 RAVENWOOD AVE MENLO PARK CA 94025-3493

1   ALLIANT TECHSYSTEMS INC
    R CARTWRIGHT
    AEROSPACE
    100 HOWARD BLVD
    KENVILLE NJ 07847

1   L MARTIN ARM SYS
    J TALLEY RM 1309
    LAKESIDE AVE
    BURLINGTON VT 05401

1   PRIMEX
    F E WOLF
    BADGER ARMY AMMO PLANT
    BARABOO WI 53913

3   PRIMEX
    E J KIRSCHKE
    A F GONZALEZ
    J DRUMMOND
    D W WORTHINGTON
    PO BOX 222
    SAINT MARKS FL 32355-0222

2   PRIMEX
    N HYLTON
    J BUZZETT
    10101 9TH ST NORTH
    ST PETERSBURG FL 33716

1   PAUL GOUGH ASSOC INC
    P S GOUGH
    1048 SOUTH ST
    PORTSMOUTH NH 03801-5423

1   FRELIN ASSOCIATES INC
    4411 QUAKER HILLS CT
    HAVRE DE GRACE MD 21078

1   GEN DYN DEF SYS (PCRL)
    N MESSINA
    PRINCETON CORPORATE PLAZA
    11 DEERPARK DR BLDG IV STE 119
    MONMOUTH JUNCTION NJ 08852

2   ROCKWELL INTRNTNL SCIENCE CTR
    DR S CHAKRAVARTHY
    DR S PALANISWAMY
    1049 CAMINO DOS RIOS
    PO BOX 1085
    THOUSAND OAKS CA 91360

1   SOUTHWEST RSRCH INST
    J P RIEGEL
    6220 CULEBRA RD
    PO DRAWER 28510
    SAN ANTONIO TX 78228-0510

1   KELLER SERVICES
    GEORGE KELLER
    3510 GARRETT COURT
    ABERDEEN MD 21001-1232

3   VERITAY TECHGY INC
    E FISHER
    R SALIZONI
    J BARNES
    4845 MILLERSPORT HWY
    EAST AMHERST NY 14501-0305

1   PRIMEX
    E STEINER
    DIR LARGE CAL R & D
    PO BOX 127
    RED LION PA 17356

1   SRI INTERNATIONAL
    TECH LIB
    PROPULSION SCIENCES DIV
    333 RAVENWOOD AVE
    MENLO PARK CA 94025-3493

    ABERDEEN PROVING GROUND

1   CDR USAATC
    STECS LI R HENDRICKSEN

28 DIR USARL
    AMSRL WM B A HORST
    AMSRL WM BE
        T MINOR
        T COFFEE
        G WREN
        C LEVERITT
        W OBERLE
        L M CHANG
        J COLBURN
        P CONROY
        D KOOKER
        M NUSCA

44

ABERDEEN PROVING GROUND (CONTINUED)

    AMSRL WM BC
        P PLOSTINS
        M BUNDY
        B GUIDOS
        D LYON
        J GARNER
        V OSKAY
        P WEINACHT
    AMSRL WM BD
        A JUHASZ
        M MCQUAID
        B FORCH
        C CHABOLOWSKI
    AMSRL WM MC
        J MONTGOMERY
        J BEATTY
        R ADLER
    AMSRL WM MB
        L BURTON
    AMSRL CI HA
        W STUREK
    AMSRL CI
        C NIETUBICZ

INTENTIONALLY LEFT BLANK.

REPORT DOCUMENTATION PAGE

Public reporting burden for this collection of information is estimated to average 1 hour per response, including the time for reviewing instructions, searching existing data sources, gathering and maintaining the data needed, and completing and reviewing the collection of information. Send comments regarding this burden estimate or any other aspect of this collection of information, including suggestions for reducing this burden, to Washington Headquarters Services, Directorate for Information Operations and Reports, 1215 Jefferson Davis Highway, Suite 1204, Arlington, VA 22202-4302, and to the Office of Management and Budget, Paperwork Reduction Project(0704-0188), Washington, DC 20503.

1. AGENCY USE ONLY *(Leave blank)*	2. REPORT DATE	3. REPORT TYPE AND DATES COVERED
	September 1999	Final, Nov 97 - Mar 98

4. TITLE AND SUBTITLE	5. FUNDING NUMBERS
An Investigation of the Erosion Physics/Mechanisms of Current Army Systems (Point Studies)	1L162618AH80

6. AUTHOR(S)

Paul J. Conroy, Paul Weinacht, and Michael J. Nusca

7. PERFORMING ORGANIZATION NAME(S) AND ADDRESS(ES)	8. PERFORMING ORGANIZATION REPORT NUMBER
U.S. Army Research Laboratory ATTN: AMSRL-WM-BE Aberdeen Proving Ground, MD 21005-5066	ARL-TR-2054

9. SPONSORING/MONITORING AGENCY NAMES(S) AND ADDRESS(ES)	10.SPONSORING/MONITORING AGENCY REPORT NUMBER

11. SUPPLEMENTARY NOTES

12a. DISTRIBUTION/AVAILABILITY STATEMENT	12b. DISTRIBUTION CODE
Approved for public release; distribution is unlimited.	

13. ABSTRACT *(Maximum 200 words)*

Future systems performance requirements have led to a heightened awareness of the erosion issue and to the development of erosion investigations in the U.S. Army and Navy. These investigations involve experimental and modeling efforts to understand the thermal, chemical, and mechanical contributions to erosion/wear. A description of the mechanistic erosion representation follows in this report. The calculation procedure is illustrated, including details of the mass transport scheme, gas-surface interface, surface melt wipe model with dynamic gridding, and the equilibrium kinetics model, which utilizes the NASA Lewis thermochemical library.

The following cartridges are investigated: the M829A2 APFSDS in the M256 120-mm tank cannon and the M791-APDS-T and 616W-APFS (the "original" M919), both in the 25-mm Bushmaster cannon. The resulting mass lost per round for these systems compares well qualitatively with the experimental data, providing some support to the assumptions in the code. The primary conclusion is that carburization leading to iron carbide formation is an important contributing factor for much of the material lost from the steel barrel once it is exposed through cracks or chips in the surface coating.

14. SUBJECT TERMS		15. NUMBER OF PAGES
gun tube erosion, heat transfer, carburization		45
		16. PRICE CODE

17. SECURITY CLASSIFICATION OF REPORT	18. SECURITY CLASSIFICATION OF THIS PAGE	19. SECURITY CLASSIFICATION OF ABSTRACT	20. LIMITATION OF ABSTRACT
UNCLASSIFIED	UNCLASSIFIED	UNCLASSIFIED	UL

NSN 7540-01-280-5500

INTENTIONALLY LEFT BLANK.

USER EVALUATION SHEET/CHANGE OF ADDRESS

This Laboratory undertakes a continuing effort to improve the quality of the reports it publishes. Your comments/answers to the items/questions below will aid us in our efforts.

1. ARL Report Number/Author_____ARL-TR-2054 (Conroy)_____ Date of Report _September 1999_____

2. Date Report Received _____

3. Does this report satisfy a need? (Comment on purpose, related project, or other area of interest for which the report will be used.) _____

_____

_____

4. Specifically, how is the report being used? (Information source, design data, procedure, source of ideas, etc.) _____

_____

_____

5. Has the information in this report led to any quantitative savings as far as man-hours or dollars saved, operating costs avoided, or efficiencies achieved, etc? If so, please elaborate. _____

_____

_____

6. General Comments. What do you think should be changed to improve future reports? (Indicate changes to organization, technical content, format, etc.) _____

_____

_____

_____

_____

Organization

_____

CURRENT   Name   E-mail Name
ADDRESS
_____

Street or P.O. Box No.

_____

City, State, Zip Code

7. If indicating a Change of Address or Address Correction, please provide the Current or Correct address above and the Old or Incorrect address below.

_____

Organization

_____

OLD   Name
ADDRESS
_____

Street or P.O. Box No.

_____

City, State, Zip Code

(Remove this sheet, fold as indicated, tape closed, and mail.)
(DO NOT STAPLE)